Electronic Supplementary Material (ESI) for Inorganic Chemistry Frontiers.

Supporting information

Prussian Blue Derived Multiple Yolk-Single Shell Structured Se-doped Fe_7S_8@NC@C Microcube Composite as a High-Rate Anode for Sodium-ion Batteries

Qingping Li, Peng Wang, Yuxiang Chen, Xiangyue Liao, Ransha Deng, Qiaoji Zheng*, Dunmin Lin*

College of Chemistry and Materials Science, Sichuan Normal University, Chengdu, 610066, P. R. China

1. Experimental

*Corresponding authors: E-mail addresses: joyce@sicnu.edu.cn (Qiaoji Zheng), ddmd222@sicnu.edu.cn (Dunmin Lin); Fax: +86 28 84760802, Tel: +86 28 84760802.

1.1. Materials

Potassium ferricyanide trihydrate [$K_4Fe(CN)_6 \cdot 3H_2O$, AR, Cologne Chemical Co., Ltd.], polyvinylpyrrolidone (PVP, K 30, AR, Aladdin Chemical Co., Ltd), sulfur powder (S, 99.95%, Adamas Reagent Co., Ltd.), selenium powder (Se, AR, Sinopharm Chemical Reagent Co., Ltd.), cetyltrimethylammonium bromide (CTAB, AR, Titan Technology Co., Ltd.), resorcinol ($C_6H_6O_2$, AR, Aladdin Co., Ltd.), formaldehyde (HCHO, AR, Sinopharm Chemical Reagent Co., Ltd), hydrochloric acid (HCl, AR, Sinopharm Chemical Reagent Co., Ltd) and ammonium hydroxide ($NH_3 \cdot H_2O$, AR, Sinopharm Chemical Reagent Co., Ltd) were used as raw materials. All chemicals were not further purified.

1.1.1. Synthesis of the PB microcubes

PB microcubes were prepared by a simple precipitation method. Typically, 11.4 g of PVP and 0.33 g of $K_4Fe(CN)_6 \cdot 3H_2O$ were added to 150 mL of 0.1 $mol \cdot L^{-1}$ hydrochloric acid solution. Subsequently, the mixture was ultrasonically dispersed for 20 min and stirred thoroughly for 10 min, and then placed in an oven at 80 °C for 24 h. After cooling, the reaction was centrifuged and washed 5~6 times with deionized water and anhydrous ethanol. The precipitate was collected and dried in a vacuum oven at 60 °C for 24 h.

1.1.2. Synthesis of the PB@RF microcubes

PB@RF microcubes were prepared by an in-situ coating route. 0.60 g PB was added into the mixed solution consisting of 18 mL of anhydrous ethanol and 42 mL of deionized water. After stirring for 30 min, 0.30 mL ammonia solution, 0.69 g CTAB,

and 0.105 g resorcinol were added to the solution and then stirred for another 30 min. 0.18 mL of formaldehyde solution was added into the above mixed solution. Finally, PB@RF microcubes were obtained after 8 h and washed with deionized water and anhydrous alcohol 5~6 times, followed by drying overnight in a vacuum oven at 60°C for 24 h.

1.1.3. Synthesis of the multiple yolk–single shell Se-Fe_7S_8@NC@C and Fe_7S_8@NC@C microcubes

Multiple yolk-single shell Se-Fe_7S_8@NC@C microcube were through a typical annealing treatment. 150 mg of PB@RF was placed downstream of the ceramic ark and 300 mg of sulfur powder was placed upstream. The ark was placed right in the middle of the tube furnace, ramped up from room temperature to 600 °C at a heating rate of 2 °C/min and held for 2 h. Nitrogen was introduced as a protective atmosphere for the annealing process. After cooling, Fe_7S_8@NC@C microcubes were obtained. Se-Fe_7S_8@NC@C microcubes were prepared in a similar procedure to that of Fe_7S_8@NC@C, with the difference that a mixture of sulfur and selenium powder (molar ratio of 2.5 : 1) was used instead of sulfur powder for the annealing treatment.

1.2. Materials characterization

X-ray diffraction (XRD, Smart Lab, Rigaku with Cu Kα radiation) was used to characterize the phase structure of the material. Field emission scanning electron microscope (FESEM/quanta250) and field emission transmission electron microscope (FETEM, G2F20, USA) were used to characterize the surface morphology and microstructure of the product. Raman spectrum was measured by a Raman spectrometer

(Renishaw RM2000, UK, 532 nm laser wavelength, 5 mW power). A field emission transmission electron microscope (TEM, Zeiss/sigma 500) equipped with an energy dispersive spectrometer was used to detect the energy dispersive spectrum (EDS). X-ray photoelectron spectroscopy (XPS, PHI 5000) was used to characterize the chemical bond and element valence of the material. Based on the principle of N_2 adsorption-desorption isotherm, Brunauer-Emmett-Teller (BET, ASAP2020HD8 specific surface area and porosity analyzer) was used to analyze the specific surface area and pore properties of the samples.

1.3. Electrochemical measurements

The anode electrode was prepared by mixing 70% of the active material (Fe_7S_8@NC@C and Se-Fe_7S_8@NC@C), 10% of polyvinylidene fluoride (PVDF) and 20% of Super P in 1-methyl-2-pyrrolidone (NMP). The copper foil was used as the collector, and the loading mass of the active material on the collector is about 1.5 mg cm^{-2}. CR2032 coin-type cells were assembled using sodium foil as the counter electrode, glass fiber membrane (Whatman, GF/A) as the diaphragm and 1M sodium hexafluorophosphate ($NaPF_6$) dissolved in DIGLYME as the electrolyte in an argon-filled glove box (O_2<0.5 ppm, H_2O<0.5 ppm). The cyclic voltammetry (CV) and electrochemical impedance spectroscopy (EIS) were tested at room temperature on CHI 760E electrochemical workstation. A constant current charge and discharge test was carried out on the automatic battery test system (LAND, CT2001A, Wuhan, China), with a voltage range of 0.01−3 V (*vs* Na^+/Na).

2. Figures

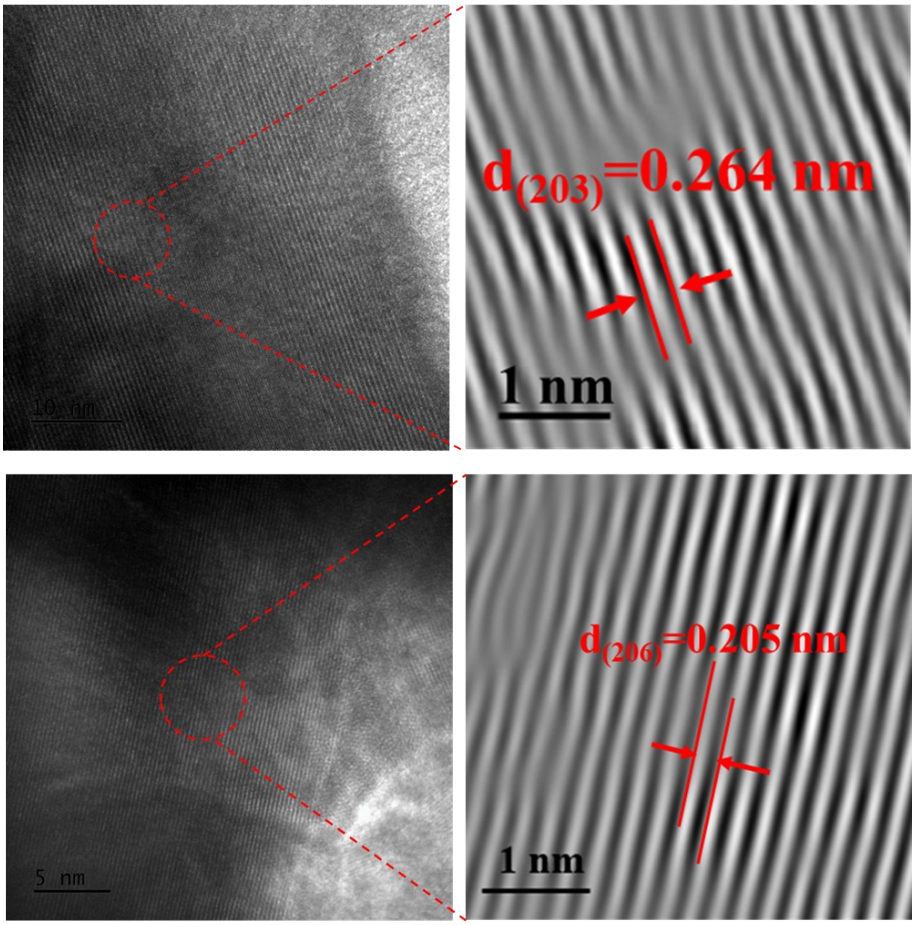

Figure S1. HRTEM images of Fe_7S_8@NC@C.

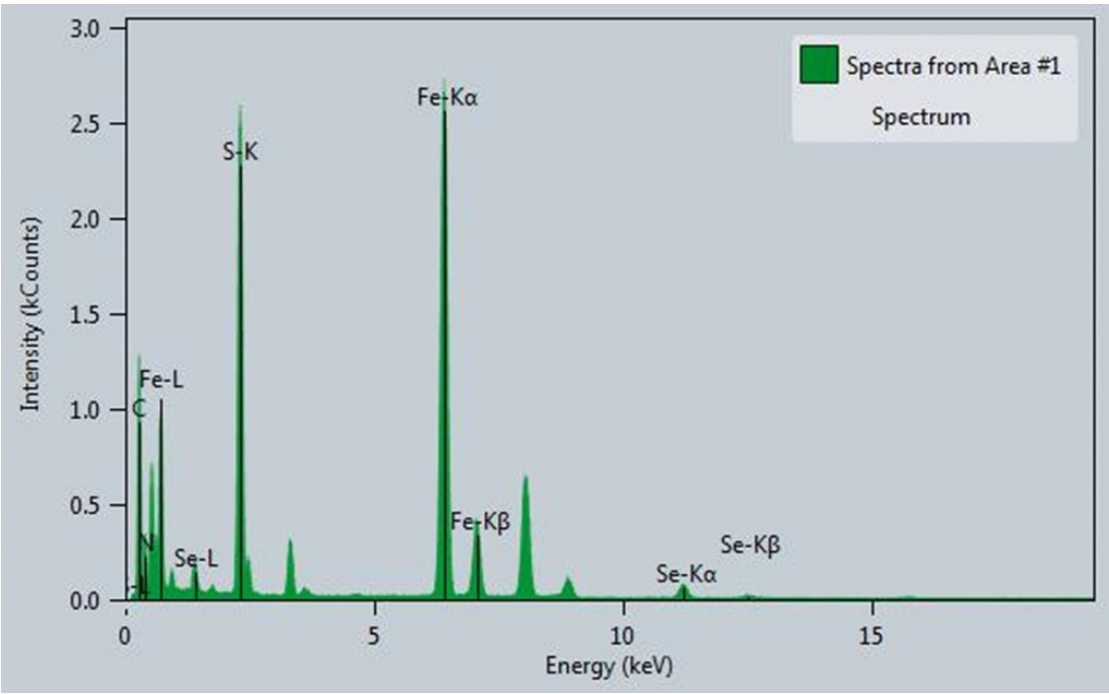

Figure S2. EDS image of Se-Fe_7S_8@NC@C.

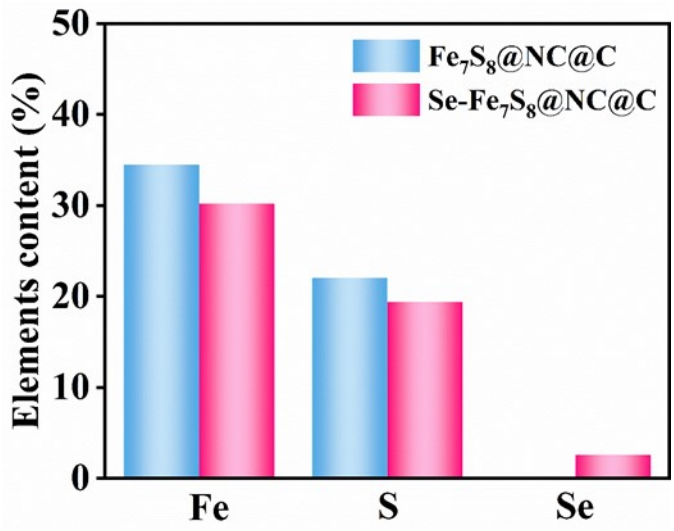

Figure S3. Elemental compositions of the materials obtained from ICP-AES test.

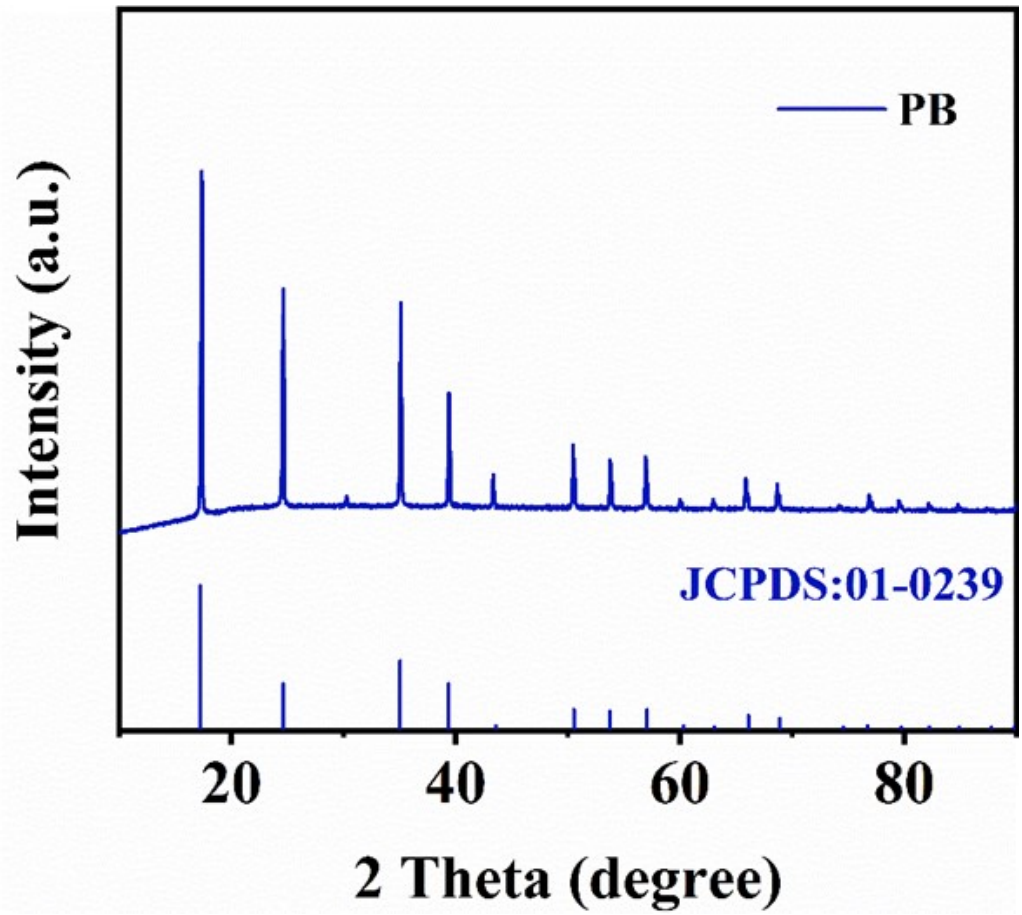

Figure S4. XRD pattern of PB.

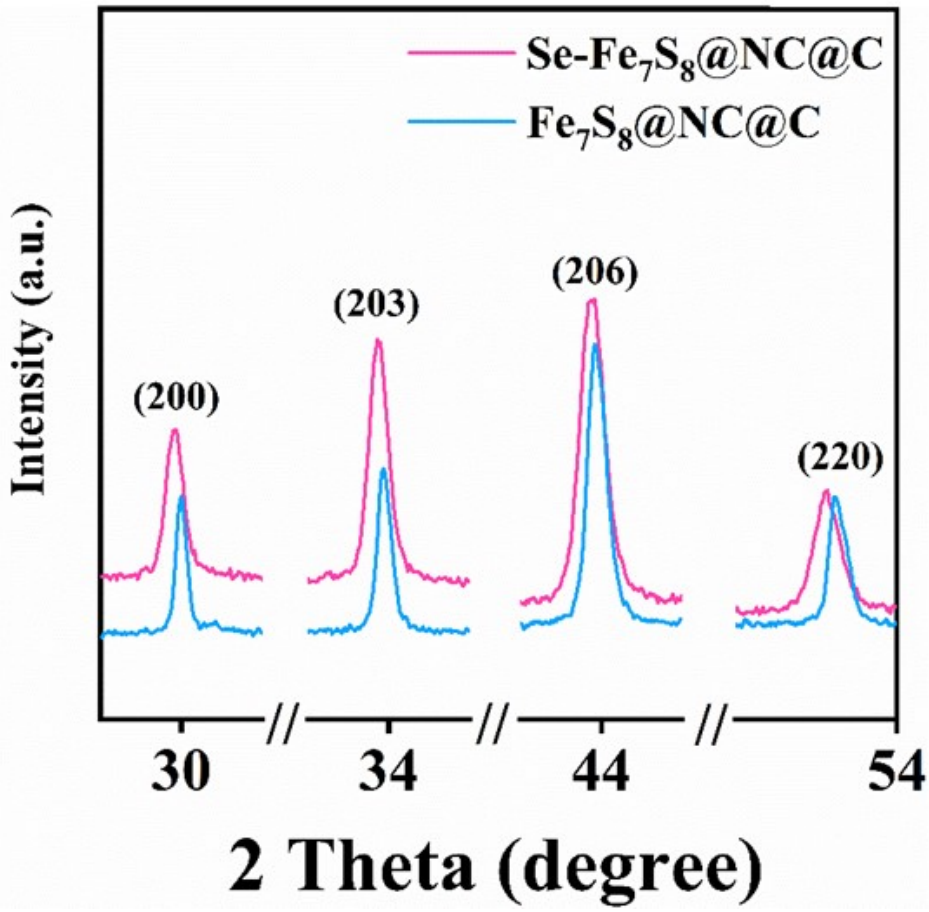

Figure S5. XRD patterns of Se-Fe_7S_8@NC@C and Fe_7S_8@NC@C.

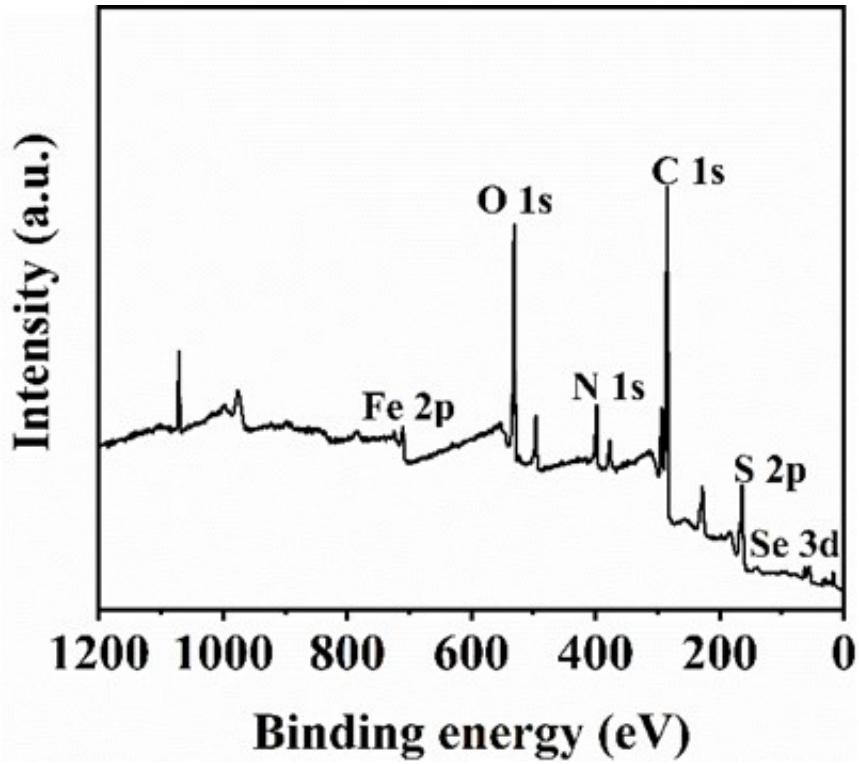

Figure S6. XPS survey spectrum of Se-Fe_7S_8@NC@C.

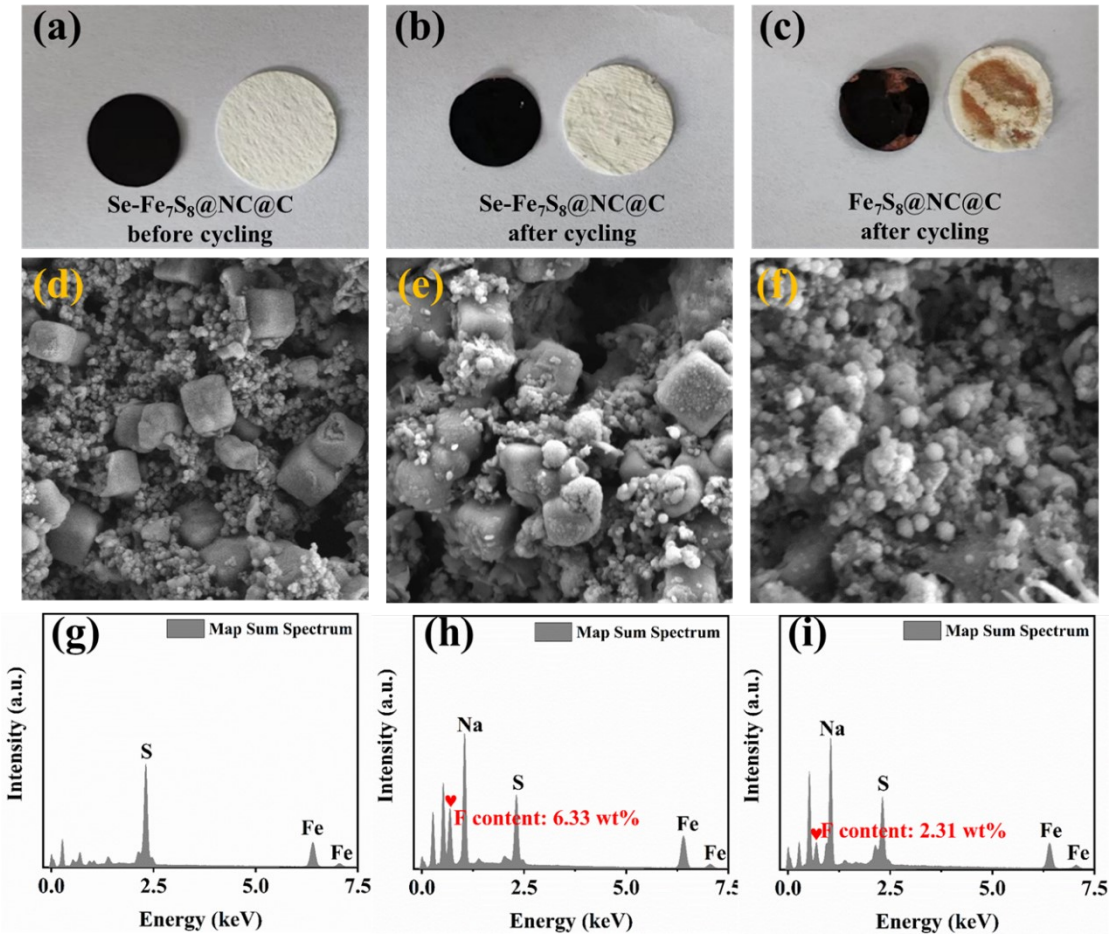

Figure S7. Photos of the (a) Se-Fe_7S_8@NC@C electrode before cycling, (b) Se-Fe_7S_8@NC@C electrode after cycling and (c) Fe_7S_8@NC@C electrode after cycling for 100 cycles at 5 A g^{-1}; SEM images of (d) Se-Fe_7S_8@NC@C electrode before cycling, Se-Fe_7S_8@NC@C electrode after cycling and (c) Fe_7S_8@NC@C electrode after cycling; EDX images of (g) Se-Fe_7S_8@NC@C electrode before cycling, (h) Se-Fe_7S_8@NC@C electrode after cycling and (i) Fe_7S_8@NC@C electrode after cycling.

Table S1. Elements atomic fraction and mass fraction of Se-Fe_7S_8@NC@C.

element	Atomic Fraction (%)	Mass Fraction (%)
C	32.93	11.93
N	5.38	2.27
S	26.66	25.79
Fe	33.63	56.66
Se	1.41	3.35

Table S2. Elemental compositions of the materials obtained from ICP-AES test.

Sample	Fe (w%)	S (w%)	Se (w%)
Fe_7S_8@NC@C	34.503	22.029	0
Se-Fe_7S_8@NC@C	30.206	19.402	2.598

Table S3. Comparison of the rate performance of recent reported sulfide anode materials with our work.

Electrode	Rate Performance Current density (A g^{-1}) / Capacity (mA h g^{-1})						Reference
Ni-WS_2/GO	0.1	0.2	0.5	1	2	5	[1]
	392	388	343	313	279	234	
Fe_2VO_4/rGO	0.1	0.2	0.5	1	2	3	[2]
	296.3	289.3	263.2	227.4	168.4	144.6	
$SnSe_{0.5}S_{0.5}$ @NG	0.1	0.2	0.5	1	2	5	[3]
	640	582	533	490	456	421	
NiS_2/$NiSe_2$ @HMCS	0.1	0.2	0.5	1	2	5	[4]
	556	473	452	420	390	353	
NiS_2@C HMs	0.2	0.5	1	2	3	5	[5]
	445.2	405.9	377.8	358.1	348.4	333.3	
MoS_2/C-VS	0.1	0.2	0.5	1	2	5	[6]
	597	566	511	469	372	276	
C-P-MoS_2 /CNTs	0.1	0.2	0.5	1	2	4	[7]
	492	482	455	427	399	360	
FeS@C	0.1	0.2	0.5	1	2	5	[8]
	504.1	480.9	463.4	452.2	435.8	394.9	
Se-Fe_7S_8 @NC@C	**0.1**	**0.2**	**0.5**	**1**	**2**	**5**	**This work**
	674.8	**641.0**	**612.8**	**585.5**	**547.4**	**448.2**	

Supplementary References:

[1] X. Luo, J. Huang, L. Cao, J. Li, Z. Xu, K. Kajiyoshi, Y. Zhao, H. Yang, Y. Liu, Z. Li, Constructing multi-dimensional migration channel by nickel-doped WS_2 composite: High speed sodium and potassium ion storage kinetics in WS_2 nanosheets, *Chemical Engineering Journal*, 2023, **464**, 142579.

[2] D. Zhao, Z. Zhang, J. Ren, Y. Xu, X. Xu, J. Zhou, F. Gao, H. Tang, S. Liu, Z. Wang, D. Wang, Y. Wu, X. Liu, Y. Zhang, Fe_2VO_4 nanoparticles on rGO as anode material for high-rate and durable lithium and sodium ion batteries, *Chemical Engineering Journal*, 2023, **451**, 138882.

[3] X. Hu, M. Qiu, Y. Liu, J. Yuan, J. Chen, H. Zhan, Z. Wen, Interface and Structure Engineering of Tin-Based Chalcogenide Anodes for Durable and Fast-Charging Sodium Ion Batteries, *Advanced Energy Materials*, 2022, **12**, 2202318.

[4] S.A. He, Z. Cui, Q. Liu, G. He, D.J.L. Brett, W. Luo, R. Zou, M. Zhu, Enhancing the Electrochemical Performance of Sodium-Ion Batteries by Building Optimized $NiS_2/NiSe_2$ Heterostructures, *Small*, 2021, **17**, 2104186.

[5] B. Cong, X. Li, G. Chen, In situ N-doped carbon nanotubes modified NiS_2 hierarchical hollow microspheres for boosting sodium storage performance, *Chemical Engineering Journal*, 2023, **460** , 141713.

[6] X. Ma, L. Diao, Y. Wang, L. zhang, Y. Lu, D. Li, D. Yang, X. She, S-vacancies manipulating enhances Na^+ insertion of MoS_2 for efficient sodium-ion storage, *Chemical Engineering Journal*, 2023, **457** , 141116

[7] X. Zhu, F. Xia, D. Liu, X. Xiang, J. Wu, J. Lei, J. Li, D. Qu, J. Liu, Crumpling

Carbon-Pillared Atomic-Thin Dichalcogenides and CNTs into Elastic Balls as Superior Anodes for Sodium/Potassium-Ion Batteries, *Advanced Functional Materials*, 2022, **33**, 2207548.

[8] D. Yang, W. Chen, X. Zhang, L. Mi, C. Liu, L. Chen, X. Guan, Y. Cao, C. Shen, Facile and scalable synthesis of low-cost FeS@C as long-cycle anodes for sodium-ion batteries, *Journal of Materials Chemistry A*, 2019, **7**, 19709-19718.